Thermochimica Acta 677 (2019) 99–108

Contents lists available at ScienceDirect

Thermochimica Acta

journal homepage: www.elsevier.com/locate/tca

Quiescent and flow-induced crystallization in polyamide 12/cellulose nanocrystal composites

Anne M. Gohn[a,d], Jiho Seo[b], Trapper Ferris[a], Priya Venkatraman[c], E. Johan Foster[c], Alicyn M. Rhoades[a,*]

[a] School of Engineering, Penn State Behrend, Erie, PA, 16563, United States
[b] Department of Materials Science and Engineering, Penn State University, University Park, PA, 16802, United States
[c] Department of Materials Science and Engineering, Macromolecules Innovation Institute, Virginia Tech, Blacksburg, VA, 24061, United States
[d] Martin-Luther-University Halle-Wittenberg, Center of Engineering Sciences, Halle/Saale, 06099, Germany

ARTICLE INFO

Keywords:
Polyamide 12
Crystallization
Cellulose nanocrystal
Fast scanning chip calorimetry

ABSTRACT

Understanding the crystallization kinetics and microstructure that result after an imposed shear flow in an additive-containing polymeric system is imperative for the development of robust polymer composites suitable for advanced engineering applications. Both nucleating agents and flow accelerate the crystallization kinetics as well as alter the ultimate polymer microstructure. During melt processing, polymers are subject to shear flow prior to the solidification of the melt. As an unsheared baseline in this study, the addition of 5 wt % cellulose nanocrystals (CNC) into quiescent polyamide 12 (PA 12) revealed that CNCs act as a natural nucleating agent to the quiescent PA 12 during slow cooling and at high temperatures, as measured by standard differential scanning calorimetry. To evaluate the role of shear work in promoting flow-induced crystallization, both neat and PA 12/CNC composite were subjected to known amounts of shear work. Then fast scanning calorimetry was used to differentiate the nucleation activity from both flow-induced precursors and CNC particles during isothermal crystallization across a wide temperature range. It was found that the addition of the CNC accelerated crystallization in the heterogeneous nucleation regime ($T > 100\,^{\circ}C$) in the quiescent material. With the addition of shear, the neat system displayed a reduced crystallization peak time with increasing shear history. In the nanocomposite system, the CNCs are an extremely efficient nucleating agent, achieving a saturating limit for nucleation of crystallization, such that shear was only a factor at low supercooling, specifically at temperatures greater than 140 °C.

1. Introduction

Polyamide 12 (PA 12) is an engineering thermoplastic that is used in diverse applications, ranging from automotive tubing and connectors to medical fabrics and bristles [1]. In recent years, the polymer has also proven to be an attractive choice for additive manufacturing, comprising the majority of selective laser sintering powders available on the market today [2]. Likewise, the polymer is increasingly adopted as filament for extrusion-based printing techniques, with several commercial options on the market [3]. Because PA 12 is a semi-crystalline polymer, the proper development of the semicrystalline microstructure is critical to yield the requisite engineering properties for application. The evenly-spaced polyamides, such as PA 12, have parallel chains in the γ-phase and antiparallel chains in the α-phase. In general, four crystal polymorphs have been reported for PA 12; α, α', γ, and γ'. It is known that the pseudohexagonal, γ-phase is the primary phase which forms at atmospheric pressure when slowly cooled from the melt [1]. However, the microstructure development is strongly dependent upon cooling conditions, and quenching from the quiescent melt induces the γ'-phase, which is also of hexagonal structure [4]. Due to the similar crystallography between γ and γ'-phases, it is often difficult to distinguish them by wide angle X-ray diffraction (WAXD). The monoclinic α-form develops when the melt is cooled under high pressures (> 500 MPa) or after drawing [1,4,5]. The monoclinic α'-phase can form at high temperatures, but transforms into the γ-phase on cooling [6]. The isothermal crystallization across the full temperature range spanning from the glass transition temperature (T_g) to the melting temperature (T_m) was recently evaluated by Paolucci et al. [7], and it was discovered that like other polyamides [8–10], PA 12 has a bimodal halftime of crystallization that corresponds to a change in nucleation

* Corresponding author.
E-mail address: amh234@psu.edu (A.M. Rhoades).

https://doi.org/10.1016/j.tca.2019.03.034
Received 27 December 2018; Received in revised form 25 March 2019; Accepted 26 March 2019

mechanism. In the low temperature regime, at temperatures less than 100 °C, PA 12 forms a mesophase, which is typical of a homogeneously-nucleated polyamide. In the high temperature regime, the γ-phase was produced between temperatures of 80 and 130 °C. At isothermal crystallization temperatures greater than 130 °C, the α'-phase was formed [7]. Drummer and coworkers recently established a link between the microstructure of PA 12 and the resultant mechanical properties; bulk samples of PA 12 crystallized in the γ'-polymorph were found to have a secant modulus 18% higher and a tensile strength 28% higher than their γ-polymorph equivalents [11].

To enhance mechanical properties of PA 12 for engineering applications, nanomaterials such as carbon nanotubes and nanofibers, halloysite nanotubes and nanofibers, and graphene nanoplatelets have been incorporated, yielding composite and nanocomposite materials [12–14]. Recently, cellulose nanocrystals (CNCs) have been incorporated into polymer systems, including PA 12, in an effort to produce enhanced polymer composite properties through the incorporation of a renewable and readily biodegradable filler [15]. For PA 12/CNC composites of 10% by weight loading, the inclusion of CNCs proved to double both Young's modulus and maximum strength relative to neat PA 12 [15]. Since the CNCs can be produced from a variety of organic materials including wood, cotton, hemp, and agricultural waste products such as nut shells [16–21], the CNCs boast a sustainable, environmentally-friendly lifetime in the polymer matrix. The physical dimensions of CNCs after acid treatment can range from 20 nm × 200–2000 nm, depending on the development procedure and source materials [22,23]. Typical nanoscale particles are known nucleating agents in the polymer melt, resulting in the acceleration of crystallization across a broad temperature range, even at high supercooling [24].

It is critical to study the crystallization kinetics of materials at process-relevant cooling and shearing rates in order to predict the consequential microstructure development. It has been established that, during injection molding, cooling rates can occur at > 600 K/s at the location where the molten polymer meets the mold wall. The polymer experiences a gradient of cooling rates through the thickness, with the lowest rates typically 10 K/s in the center of a molded part [25]. Rapid cooling rates drive crystallization to occur at low temperatures. In addition to the rapid cooling, the polymer also undergoes shear flow prior to crystallization in both injection molding and fused filament additive manufacturing. Shear rates in the cavity of an injection molded part have been reported to range from 8,000 to 15,000 s^{-1} [26], but the duration of the high shear may be as short as a fraction of a second during mold filling. During the fused filament extrusion additive manufacturing processes, the shear rates are much lower and typically range between 100–200 s^{-1} [27]. These conditions play a key role in the microstructure development, and further understanding the crystallization kinetics after the melt experiences these conditions can help to predict final polymer microstructure, which drive ultimate bulk properties.

Polymers crystallized after shear flow display several differences relative to their quiescently-crystallized equivalents. The additional energy and polymer orientation that results from shear flow will yield, in the solidified polymer, an increased number of crystal nuclei and an oriented microstructure, accelerated crystallization kinetics, and crystal precursors that display an increased lifetime at temperatures below the equilibrium melting temperature (T_m^0) [28]. To quantify the influx of energy to the polymer due to shear flow, a specific work (W) term is often adopted [29–32]. This specific work drives the development of flow induced precursors that affect subsequent crystallization processes [33,34]. While many studies focus on the individual influence of shear rate, shearing time, or shear stress, it is the combination of these factors that give comprehensive information on the flow strength developed in sheared polymers. In this study the specific work was calculated for all samples of interest, and each sample will be referenced according to the specific work to which it was subjected in the melt. The specific work introduced in the sample is the product of the shear stress (σ) and the shear rate ($\dot{\gamma}$) experienced by the polymer. Experimentally, shear stress is represented by parameters of viscosity (η), shear rate, and shearing time (t_s), as shown in Eq. (1).

$$W = \sigma\dot{\gamma} = \eta\dot{\gamma}^2 t_s \quad (1)$$

In previous work with polyamide 66, it was determined that the flow-induced precursors were sufficiently stable such that they would repeatedly nucleate crystallization in the sample after several melt-quench cycles in fast scanning calorimetry, provided that the melting temperature remained lower than the equilibrium melting temperature. This approach was used to obtain crystallization kinetics at process-relevant cooling rates and temperatures [35]. In this study, the same methodology was applied to a PA 12/CNC nanocomposite in order to establish nucleating influence of both the CNC particles and shear flow, and to determine if the nucleating influence of shear is intensified or overshadowed by the nucleating effects of the nano-additive.

2. Experimental

2.1. Materials

The PA 12 used for this evaluation was purchased as a fused deposition modeling filament from Rigid Ink due to its interesting properties related to the additive manufacturing community. The material supplier of this resin is Evonik Industries (Essen, Germany). This PA 12 has a glass transition temperature (T_g) of 45 °C and a melting temperature (T_m) of 178 °C, which is lower than most nylons [1]. The equilibrium melting temperature (T_m^0) of PA 12 is 187–190 °C [36,37]. No additives were found in the material, as characterized by proton and Carbon 13 nuclear magnetic resonance spectroscopy. Both spectra showed only peaks from PA12 resin and peaks from the extraction solvent. Gas Chromatography / Mass Spectroscopy was also used to confirm that no additives were present in the as-received PA 12. As outlined in the Supplemental Information, the peak-time of crystallization of the PA 12 used in this study was greater than those reported for a low molecular weight PA 12 [7], indicating that the molecular weight of this PA 12 was greater than that of the EOS PA2200 employed in the referenced work.

Cellulose nanocrystals (CNCs) were obtained as freeze-dried product from Forest Products Lab (FPL) (sulfuric acid hydrolysis, from wood pulp; 0.94 wt% sulfur content on dry CNCs). A Brabender torque rheometer with mixing chamber was used to compound the PA 12 + 5% CNC material batches. Compounding was performed at 200 °C for 5 min at 50 RPM mixing speed. The composite was then taken from the Brabender and hot pressed to form a flat, 1 mm thick specimen using a Carver press at 200 °C.

2.2. Instrumentation

2.2.1. Nuclear magnetic resonance (NMR)

To confirm no additives were present that could nucleate the base polymer resin, NMR was employed to analyze the dissolved as-received PA 12. Approximately 28 mg of the PA 12 resin was placed in a mixture 0.2 mL trifluouroacetic acid and 2 mL of deuterated chloroform. The extract was analyzed using a Bruker Avance II 400 MHz spectrometer. A 16 scan proton spectrum and a 1024 scan Carbon 13 spectrum were obtained.

2.2.2. Gas chromatography–mass spectrometry (GC–MS)

The extract prepared for NMR was also injected in to Hewlett Packard 6890 gas chromatograph with a 5972 mass selective detector. The procedure was programmed from 50 to 280 °C at a heating rate of 6 K/min. The separation was performed on a 30 m × 0.25 mm column (0.25 μm film thickness). The mass spectrometer employed electron impact ionization and a scan mode of 50 m/z to 500 m/z.

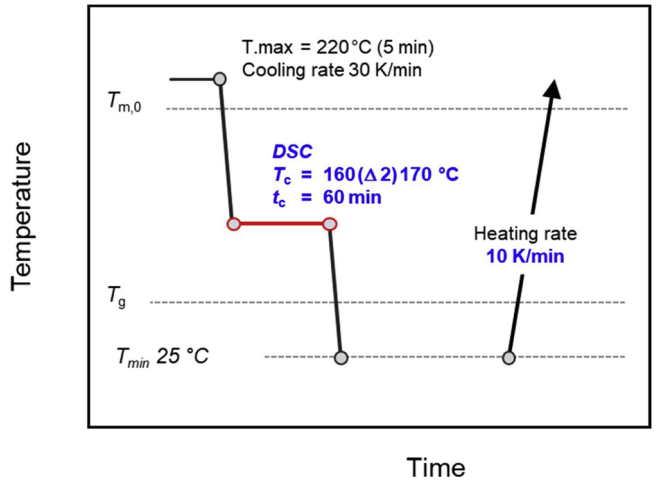

Fig. 1. Standard DSC method for high temperature isothermal crystallization between 160 and 170 °C.

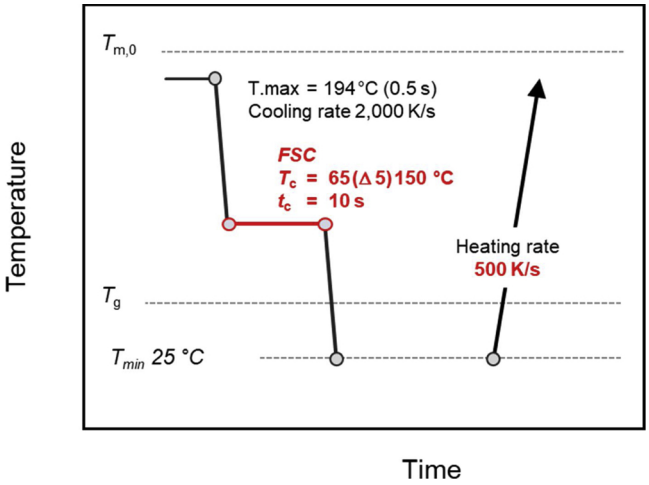

Fig. 2. Fast Scanning Calorimetry method for determining peak time of crystallization in PA 12 and its composites. The maximum temperature in the method was limited to 194 °C to ensure the shear history in the specimen was not erased.

2.2.3. Particle size analysis

The particle size of the as-received CNC was established by homogenizing the 0.1% cellulose aqueous suspension by IKA T25 digital Ultra Turrax. Then dynamic light scattering was carried out using a Zetasizer Nano ZS.

2.2.4. Parallel plate rheometry

To systematically study the effects of shear at known levels of specific work, parallel plate rheometry was employed for sample preparation. An ARES-G2 rheometer (TA Instruments, New Castle, DE) equipped with 8 mm stainless steel parallel plate fixtures was used to fabricate the shear discs. All neat and composite PA 12 samples were dried in a vacuum oven at 80 °C overnight to minimize moisture effects. Prior to loading the material, Kapton tape was attached to the top and bottom plates to facilitate easy removal of the sheared disc after solidification [38]. The sheared discs were then preserved for subsequent X-ray and calorimetric analyses. The geometry gap between plate and plate was ~0.9 mm (without Kapton tape thickness) for both neat and 5% CNC / PA 12 samples. The Kapton film thickness was ~0.05 mm (~50 μm). The PA 12 disc thickness was ~0.9 mm which was slightly thinner than the geometry gap due to densification during crystallization.

A time-temperature protocol that employed both steady and oscillatory shear was developed for the sheared-disc fabrication. The plates were heated to 190 °C, where the sample was loaded and held for 1 min to fully melt. A constant shear rate of about 0.5 s^{-1} was then applied to the molten pellets for 3 min to aggregate the pellets to rid the melt of any air bubbles. To erase any shear history in the materials from the pelletizing or compounding methods, the material was held at 220 °C without shearing for an additional 2 min. After the annealing step, the melt was cooled at 10 K/min to 190 °C, held for 3 min to achieve a constant temperature, then it was sheared for 1 min at 100 s^{-1}. Once shearing was complete, the samples were cooled to room temperature at 10 K/min. The solidified material was then taken from the instrument for subsequent analyses.

The shear history, which influences crystallization kinetics, is defined by both shear rate and shear time. To quantitatively investigate the combination of these variables on the flow-induced crystallization kinetics, the applied specific work model described in Eq. (1) was used. As explained by Janeschitz-Kriegl et al. [39], the shear-rate dependent viscosity, $\eta(\dot{\gamma})$, can be obtained from rheological shear thinning models. In this study, Cross model was adopted to systemically determine $\eta(\dot{\gamma})$. Assuming that the shear rate is linearly proportional to the disc radius, the applied specific work was calculated at each point of interest along the disc radius. After the polymer experienced these known shear conditions, the sample was removed from the rheometer and sectioned for subsequent crystallization studies.

2.2.5. X-ray diffraction (XRD)

Wide-angle XRD measurements were performed on a Malvern Panalytical Empyrean Series 3 system using a Cu radiation source and a GaliPIX3D CdTe area detector. The analysis was done in transmission mode. A 300 μm monocapillary incident optic produced a 500 μm spot

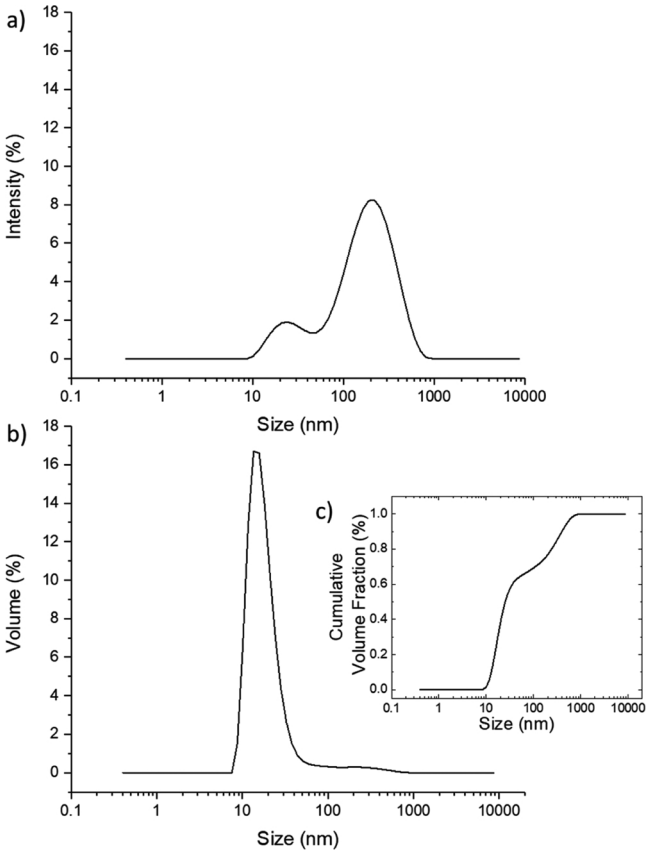

Fig. 3. Particle size analysis of CNC as-received prior to melt processing. Analyses showing intensity (a), volume (b), and cumulative volume fraction (c) are displayed. Peak intensities are displayed at approximately 24 and 220 nm.

size on the sample. The measurements were taken at 45 kV and 40 mA for 75 s. The 2D image was analyzed using XRD2DScan software (Malvern Panalytical).

2.2.6. Differential scanning calorimetry (DSC)

A standard DSC1 from Mettler-Toledo with a Thermo Scientific EK90/MT intracooler was used to collect isothermal and non-isothermal crystallization data of the quiescent materials. All measurements were performed under nitrogen purge gas, with samples of approximately 5 mg loaded into a 40 µL aluminum pan with pierced lid. A non-isothermal analysis was performed by heating the sample at 10 K/min to 220 °C, where it was held for 5 min. The sample was then cooled at the specified rate to 25 °C, where it was held for 5 min and then the cycle was repeated until all cooling rates were analyzed. The cooling rates studied in this experiment include 5, 10, 20, and 30 K/min.

Isothermal crystallization experiments of the unsheared samples were carried out by first heating the sample to 220 °C for 5 min to erase any previous shear history in the material, followed by cooling to the target crystallization temperature where the exotherm was monitored as a function of time using standard DSC. For sheared samples, the maximum temperature of the melt used was 194 °C, because this temperature is below the reported equilibrium melting temperature of PA 12. A maximum temperature of 194 °C was also used to stay consistent with the degree of supercooling used in the FSC experiments. The method is detailed in Figure 1.

Fast scanning chip calorimetry (FSC)

The equipment used was a power-compensating Mettler-Toledo Flash DSC 1 with a Huber intracooler TC100. Prior to sample evaluations, the empty sensor was conditioned and temperature-corrected per specifications of the instrument provider. The sensor environment was purged with ultra-high purity nitrogen gas at a flow rate of 60 mL/min to avoid sample oxidation and prevent atmospheric moisture in the sample chamber. Specimens were prepared by microtoming the as-received pellets to a 12 µm thickness, then cutting laterally with a scalpel under a stereo microscope to achieve approximately a 100 µm × 100 µm square. A thin layer of Wacker AK 60,000 silicon oil was painted between the sample and sensor membrane to improve thermal contact. The method used for FSC is detailed in Figure 2.

2.2.7. Polarized-light optical microscopy (POM)

The molded samples were imaged employing a Leica DM2700 P microscope equipped with a Leica DFC 7000 T camera. Prior to sample imaging, both the neat PA 12 and the PA 12 / CNC composite were annealed at 165 °C for one hour and slowly cooled to room temperature. For imaging, samples were cut to a thickness of 10 µm using a rotary microtome equipped with a tungsten carbide knife Fig. 1 , Fig. 2 .

2.2.8. Atomic force microscopy (AFM)

AFM measurements were performed using a Bruker Dimension Icon. Samples were conditioned at 160 °C [8]. PeakForce tapping imaging mode was used with a ScanAsyst Air Probe (0.4 N/m spring constant). Image analysis was done using Nanoscope Analysis software. To approximate lamellae thickness, 20 measurements were randomly selected to determine the average thickness.

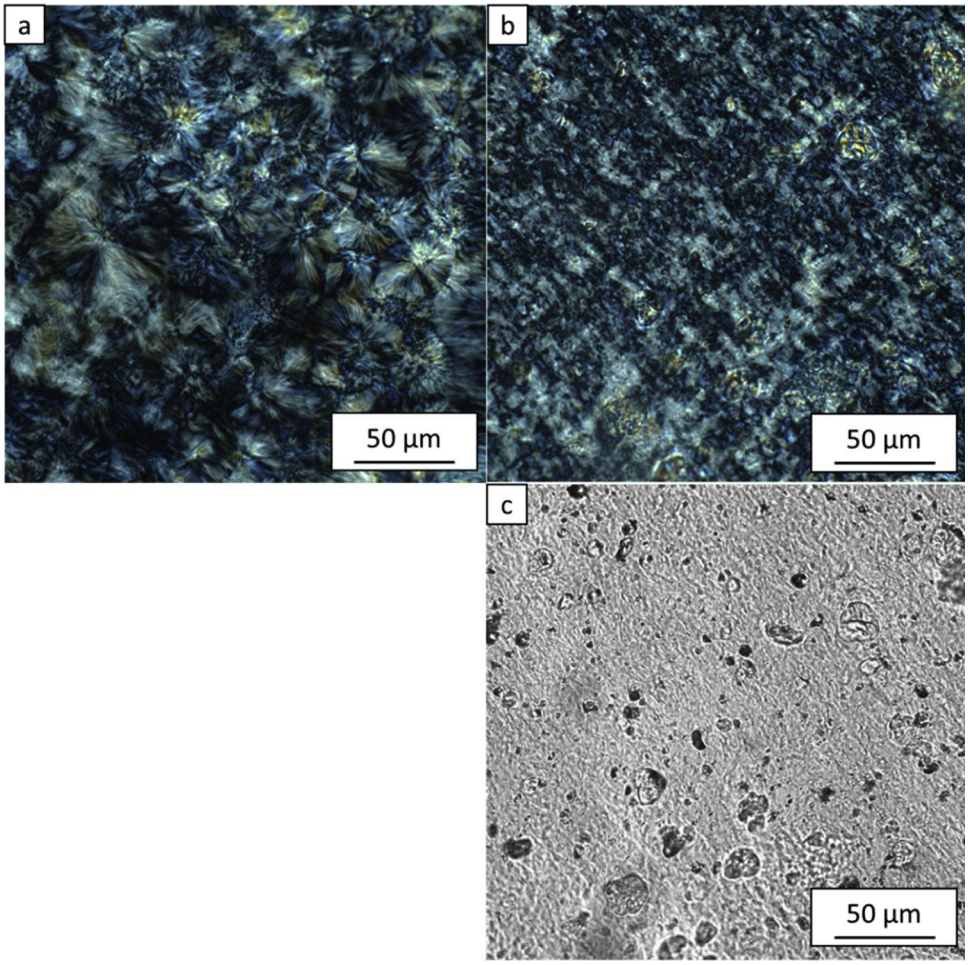

Fig. 4. Polarized light microscopy images of the neat PA 12 polymer (a) and PA 12 / CNC composite (b) after slow cooling of the melt. An image of the same nucleated sample (b) in transmission without polarizers is also displayed in (c) to show CNC agglomerates that are present in the material.

3. Results and discussion

Prior to melt mixing, the particle size distribution of the CNCs was established using dynamic light scattering. The intensity and volume plots are displayed in Fig. 3. While there is a population of large (> 10 μm) particles that can be seen in microscopic images in Fig. 4, analysis confirmed that 90% of the particles by volume are less than 400 nm in size, and 70% of particles are less than 100 nm. Therefore, we expect the thermal analysis of the composite to be dominated by the nanoparticles confined within the polymer matrix. This nano-filler nucleating behavior is evidenced by FSC analysis where the composite sample size is < 100 ng, which is too small to accommodate large CNC agglomerates.

While a homogenous, agglomerate-free composite was desired, it is not surprising that such particle distribution was not achieved during melt-mixing. Torkleson and coworkers have determined that, in order to produce a homogenous distribution of CNC without agglomerates in polyolefins, solid state shear pulverization techniques must be used [40]. However, a fraction of nanoparticles was distributed in the matrix and it is these nanoparticle-rich regions from which samples were extracted for FSC crystallization kinetic studies. The semicrystalline microstructure obtained on slow cooling after annealing at 165 °C is shown in Fig. 4. Polarized light microscopy images of the neat PA 12 polymer (a) and PA 12/CNC composite (b) after slow cooling of the melt are shown in Fig. 4. The neat material forms large spherulites of about 30 μm in diameter, while the composite PA 12/CNC material has a much finer crystalline microstructure of much higher nucleation density. Large CNC agglomerates are observable in Fig. 4(b), but no crystal growth is observed from the surface of the CNC agglomerates.

Standard DSC studies of the neat PA 12 and PA 12/CNC composite reveal the strong nucleating effect of the CNCs in the quiescent polymer. As shown in Fig. 5, both the neat and the nucleated materials were subjected to high temperature isothermal crystallization ranging between 160 and 170 °C. It is shown that the isothermal crystallization of unfilled PA 12 could only be quantified up to temperatures of 166 °C. At higher temperatures, the crystallization rate was too slow to produce a detectable calorimetric signal. However, the PA 12/CNC composite was able to crystallize at temperatures up to 170 °C. At 160 °C, the peak time of crystallization for the neat material was 294 s, while the peak time of the PA 12/CNC composite was only 87 s, a reduction of about a third of the time required for crystallization, indicating a significant nucleating effect of the CNCs in the system.

The non-isothermal crystallization behavior for these materials are displayed in Fig. 6. Fig. 6(a) displays the crystallization on cooling for the neat material, while Fig. 6(b) shows that of the composite material. The cooling rates analyzed in the standard DSC include 5, 10, 20, and 30 K/min. As is typical in DSC experiments, with increasing cooling rate, the crystallization temperature is suppressed to lower temperatures. At the lowest rate, 5 K/min, the neat PA 12 has a peak

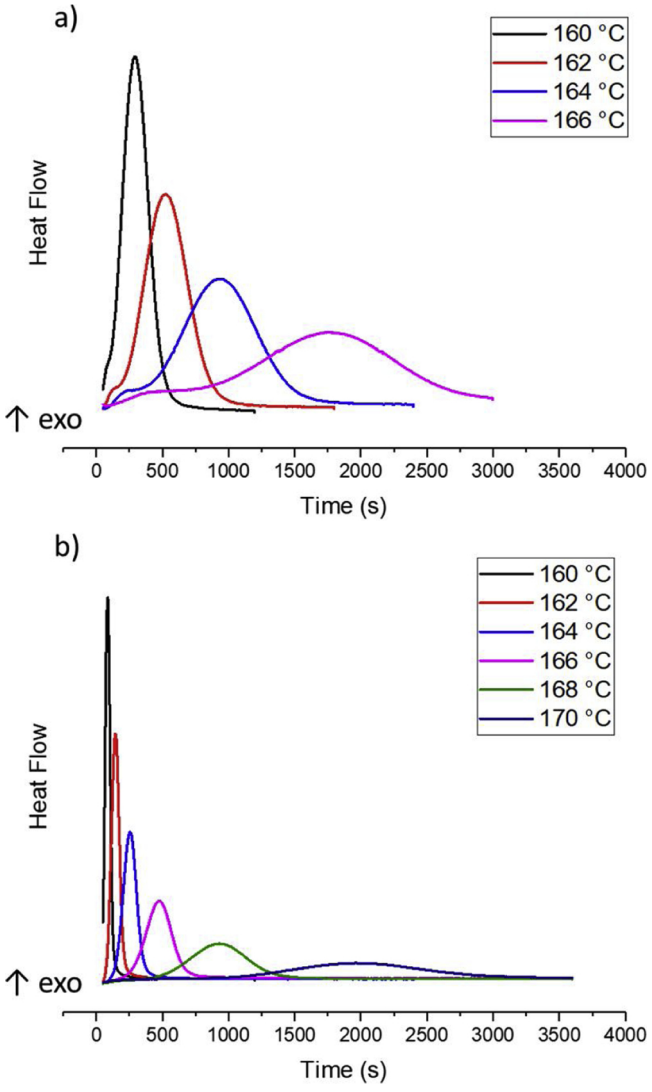

Fig. 5. Isothermal crystallization of neat (a) and CNC composite (b) PA 12 using standard DSC between 160 and 170 °C.

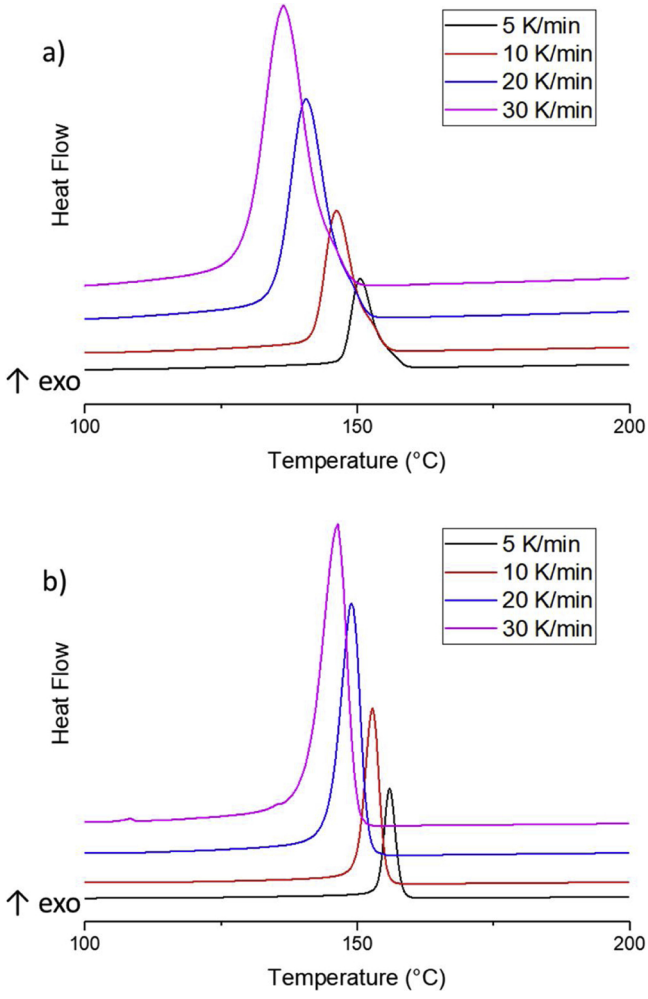

Fig. 6. Non-isothermal crystallization of neat (a) and CNC composite (b) PA 12 using standard DSC between 5 and 30 K/min.

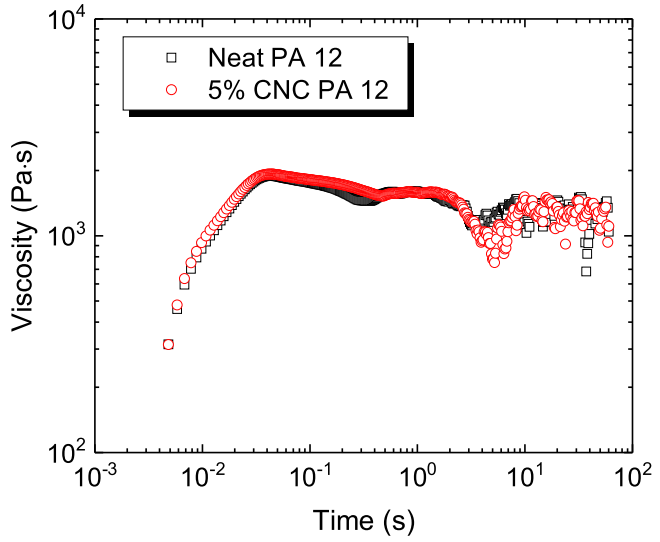

Fig. 7. PA 12 and PA 12/CNC viscosity as a function of time at 190 °C with a shear rate of 100 1/s applied at the outer edge; measurement taken during the shearing preparatory step in making the sheared disc for FSC analysis.

crystallization temperature (T_c) of 150.6 °C and the nucleated has a T_c of 155.9 °C, resulting in a 5.3 K difference. At the maximum rate, 30 K/min, the neat PA 12 has a T_c of 136.3 °C, while the nucleated has a T_c of 146.1 °C, resulting in a 9.8 K difference. It is apparent that the CNC additive has a strong effect on non-isothermal crystallization at low cooling rates, but is more pronounced at higher rates. The nucleated system also is less dependent on cooling rate, as its T_c only shifts 9.8 K within this cooling range, while the neat material is more easily influenced, shifting 14.3 K depending on the cooling rate used in this range.

The objective of this study is to differentiate between the nucleating influences of both CNC nanoparticles and shear flow in PA 12. Therefore, after initial thermal characterization, both the neat and composite PA 12 materials were subject to parallel plate rheology in order to a) establish the rheological properties of each composition and b) introduce a known amount of shear work into the materials in order to create flow-induced crystallization and the resulting FIC microstructures. Polymer crystal microstructure formed under flow is known to contain chain-extended structures that survive in the melt at temperatures less than T_m^0, and therefore these sheared samples, or samples prepared using parallel plate rheometry, were preserved after viscosity measurements for subsequent thermal analysis using FSC. As shown in

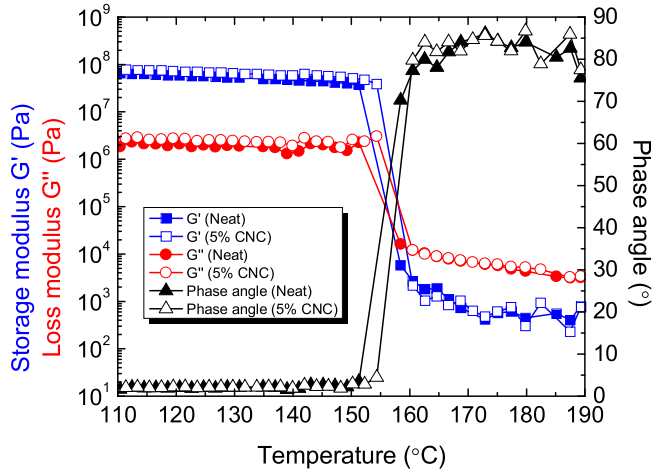

Fig. 8. Storage modulus and loss modulus as a function of temperature on cooling at 10 K/min.

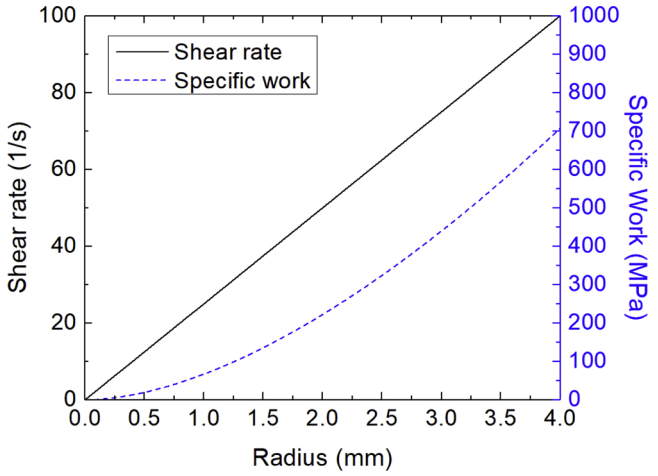

Fig. 9. Shearing conditions of each disc. The total shear rate at the edge for each disc was held constant at 100 s^{-1} for 1 min.

Fig. 7, both the neat PA 12 and the PA 12/CNC composite displayed very similar rheological behavior at 190 °C, with a shear rate of 100 1/s applied at the outer edge. Typically, it would be expected that the nanocomposite would yield a higher viscosity [41], but in this case the CNC does not significantly affect the rheological behavior of PA 12 at high temperatures because the PA 12 viscosity is so low that the effect of the CNC is presumably negligible. Also shown in Fig. 7, the x-axis represents shearing time in log scale. Thus, the degree of fluctuation

Table 1
Summary of specific work and shear rate for sampling locations across the disc. The center of the disc, where shear rate, and thus, specific work, should be 0, is designated as 0* because drag forces are still imparted on the center of the disc, and therefore not truly a shear-free state.

Disc Position	Shear Rate	Specific Work
Unit	s^{-1}	MPa
Center	0*	0*
1 mm from Center	25	50
2 mm from Center	50	200
3 mm from Center	75	400

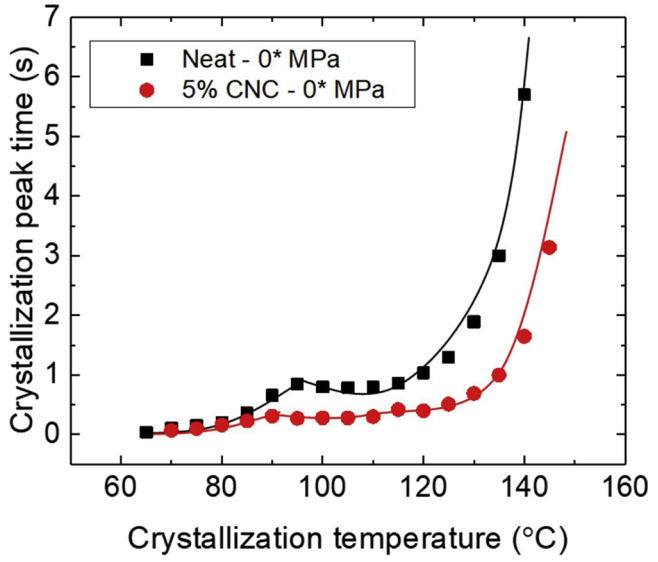

Fig. 10. Peak time of crystallization at 0* MPa comparing the neat and CNC composite material. The lines are a guide for the eyes.

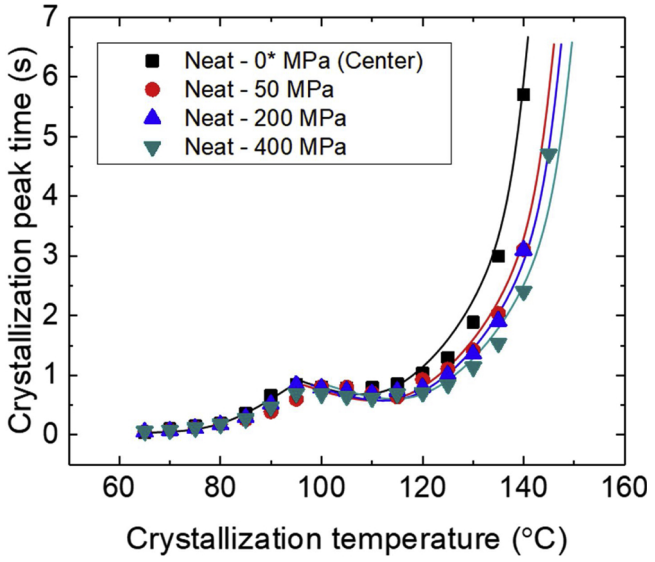

Fig. 11. Peak time of crystallization for neat PA 12 at increasing levels of shear work. The lines are a guide for the eyes.

increases at longer times. Weak edge fractures could also induce the fluctuation and cause a decrease in viscosity at long shearing times. Since the viscosity of the polymer and composite are required to calculate the specific work (*W*) of flow, both the neat and CNC composite PA 12 samples had similar viscosity contributions at each location used for FSC analysis.

During melt crystallization, the viscosity and modulus increase because of the space-filling and subsequent physical network formation with the crystallites [42]. The crystallization kinetics can be monitored by conducting oscillatory temperature sweep [38]. Fig. 8 shows the dynamic modulus evolution of sheared PA 12 with and without CNC as a function of temperature on cooling at 10 K/min. Prior to the cooling, identical shear rate of 100 s^{-1} and shearing time of 1 min were applied to both neat and PA 12/CNC. The sheared CNC composite PA 12 shows ~ 5 K higher crystallization temperature than that of neat PA 12 presumably due to the higher nucleation rate by CNC. This result is confirmed by the DSC cooling rate analysis displayed in Fig. 5, where under controlled cooling at 10 K/min, crystallization in the nucleated specimen occurred 7 K higher than in the neat PA 12. The composite material also shows slightly higher storage and loss modulus at all temperatures, presumably to the composite composition.

Since the sheared PA 12 discs with and without CNC were fabricated using 8 mm parallel plates, the sheared discs had a range of shear rates from ~0 s^{-1} to at the center to ~100 s^{-1} at the perimeter. After forming on the parallel plate rheometer, both the neat and polymer composite discs were removed from the rheometer and then sectioned to obtain access to the desired radial location on the disc. At this location, the disc was microtomomed to obtain a 10 µm slice that isolated the polymer at the specific radial location. This 10 µm slice was then laterally cut with a scalpel to obtain samples appropriately sized for FSC analysis [35]. Fig. 9 shows the calculated shear rate and specific work as a function of the radius, as detailed in Fig. 8. The specific shear rates and work levels for sampling locations are listed in Table 1. Sampling for FSC measurements was limited to 3 mm from the center of this disc in order to eliminate any effects of edge fracture that may have occurred during the creation of the samples, as indicated by Fig. 7.

Fig. 10 shows the peak time of crystallization for both the neat and composite PA 12, with a sample obtained from the center of each sheared disc, where minimal shear history was imparted on the melt. The peak time curve displays a bimodal peak time of crystallization, which has been proven to relate to the change in nucleation

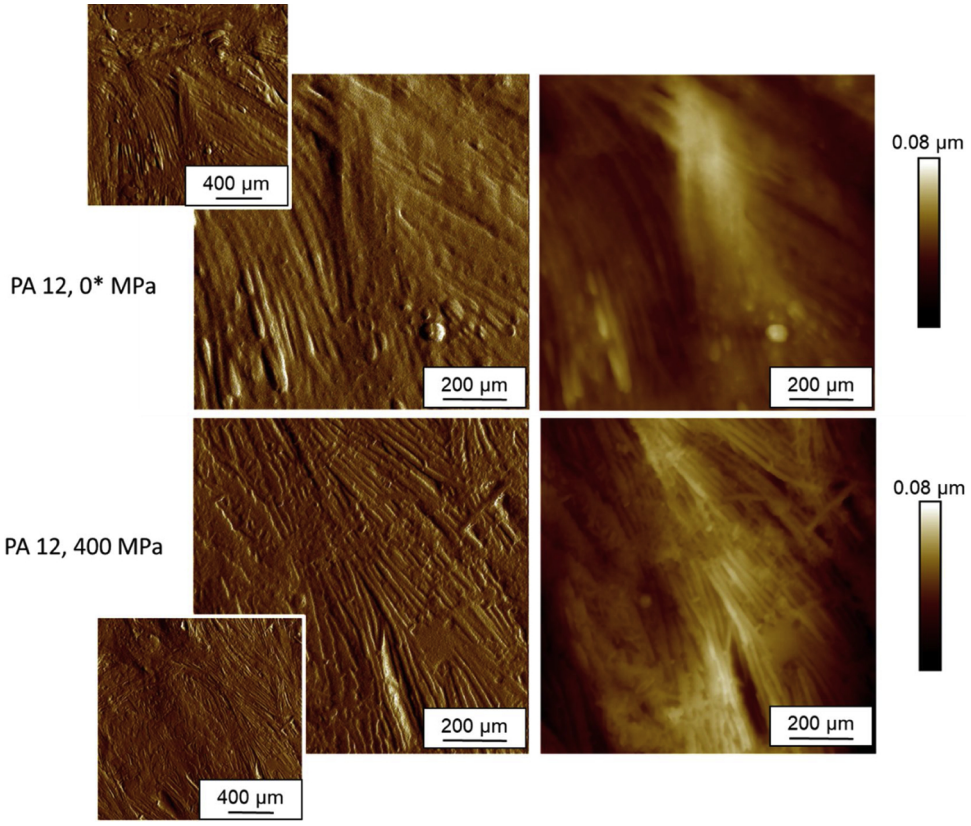

Fig. 12. AFM images of samples of neat PA 12 isothermally crystallized at 160 °C after specific shearing conditions. Top row images show the disc center and bottom row images show the disc edge. Images to the left represent error mode scans and the right show height mode.

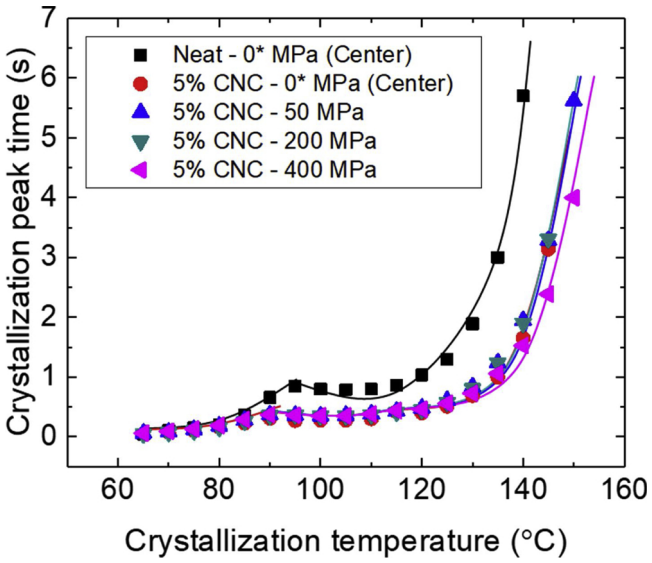

Fig. 13. Peak time of crystallization for PA 12/CNC at increasing shear work levels. The lines are a guide for the eyes.

mechanism; the low temperature regime, shown here between 60 and 85 °C, corresponds to homogeneous nucleation in polyamide 12 [7,43]. Between 85 and 95 °C, nucleation changes to a heterogeneous mechanism, where a high temperature peak is displayed. FSC was able to provide peak time data up to 145 °C for these specimens.

Both the neat and CNC composite PA 12 show an identical peak time of crystallization in the homogeneously nucleated regime, while crystallization is accelerated in the heterogeneous nucleation regime. At 140 °C, the peak time of crystallization of the neat PA 12 is 5.7 s, where the peak time of the CNC PA 12 nucleated system is 1.65 s. This behavior of heterogeneous nucleation is in accordance with unsheared polyamide 11 composite systems characterized using FSC [44] and the systems established by Christoph Schick and coworkers such as poly(ε-caprolactone) [45] and poly (butylene terephthalate) (PBT) [46]. For comparison, the peak time of crystallization of PA 12 from Paolucci and coworkers [7] is presented in the Supporting Information. Compared to the work of Paolucci, this grade of PA 12 displays slower crystallization, confirming the known behavior of an increased molecular weight [47].

Fig. 11 displays the peak time of crystallization across the neat, sheared disc. Again, the specific work values listed in the legend correspond to samples taken at 1 mm (50 MPa), 2 mm (200 MPa), and 3 mm (400 MPa) from the center of the specimen in the direction of flow. Similar to the results displayed in Fig. 10, the homogeneous nucleation regime maintains a consistent peak time of crystallization regardless of the shear history imparted on the specimen. However, in the heterogeneous nucleation regime, the shear flow develops crystallization precursors that act as nucleating agents, resulting in a decrease in crystallization time. It is shown that even at a specific work value of 400 MPa, the peak time of crystallization is still decreasing, indicating that the work level has not yet reached a saturation limit in the material.

To further establish the effects of shear on the resulting crystallization, AFM images were collected to more closely examine the microstructure of the materials. Specimens were collected at 0* MPa and 400 MPa locations in the discs and annealed prior to imaging at 160 °C [8]. Fig. 12 shows the resulting images of the neat disc at the center

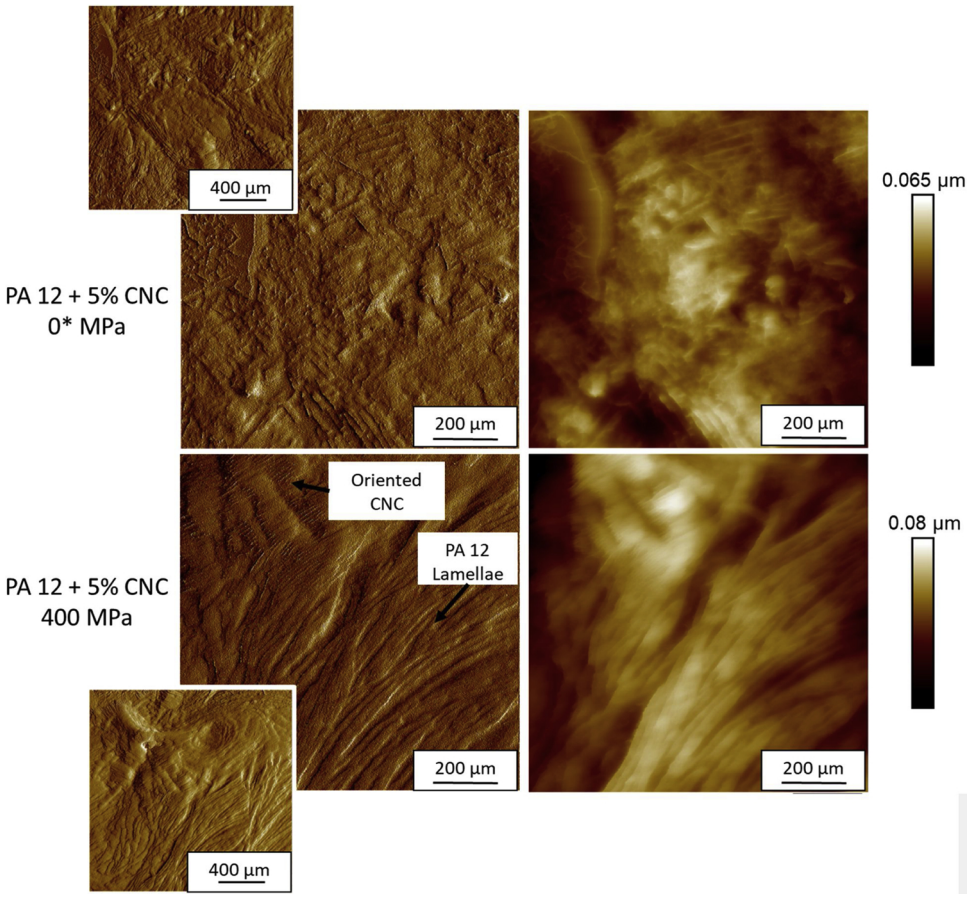

Fig. 14. AFM images of samples of PA 12/CNC isothermally crystallized at 160 °C after specific shearing conditions. Top row images show the disc center and bottom row images show the disc edge. Images to the left represent error mode scans and the right.

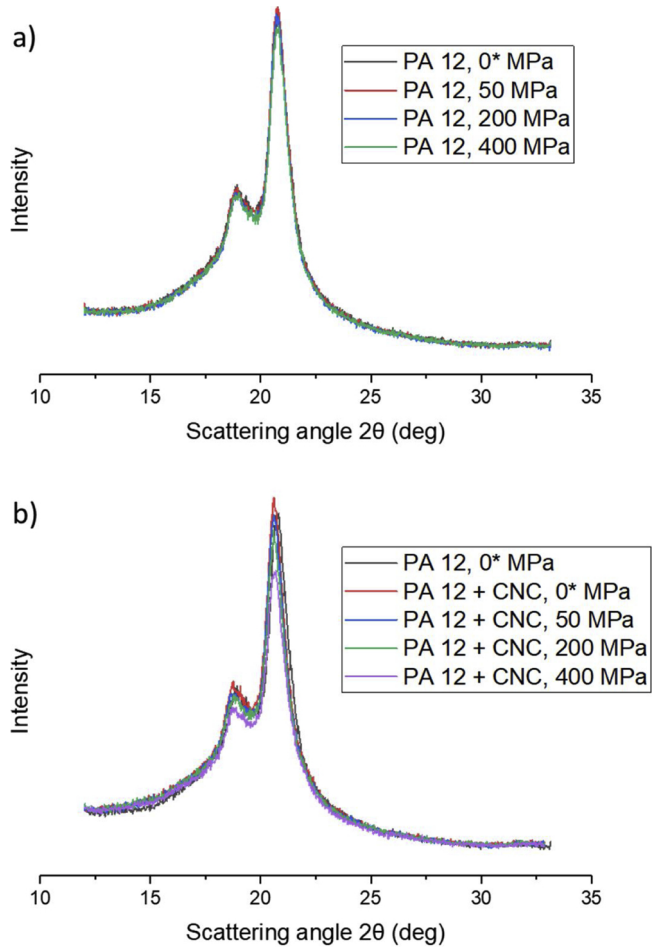

Fig. 15. XRD patterns of PA 12 (a) and PA 12/CNC (b) with increasing shear history.

(top row) and 400 MPa (bottom row). Images are displayed in both error mode (left) and height mode (right). It can be seen that the PA 12 crystallized in the center of the disc is able to form large lamellae, nucleating from a specific point and fanning into a spherulitic geometry. However, after the neat PA 12 is subject to 400 MPa shear work, it produced lamellae that do not have distinct nucleation points or spherulitic geometry. The lamellae in the neat material at the center of the sheared disc have an average width of 25 ± 4 nm, and the lamellae at the edge of the disc, corresponding to 400 MPa, have lamellae ranging from approximately 18 ± 3 nm in width.

The peak time of crystallization for the sheared, nucleated material is presented in Fig. 13. As already discussed, the nucleated material crystallizes faster than the neat material in the heterogeneous nucleation regime. Interestingly, though, the nucleated material is not strongly influenced by shear history. Only at the very high crystallization temperatures (> 140 °C), does the shear history influence the crystallization time. It appears that the CNCs are able to nucleate the PA 12 to a saturation point that even imposing shear cannot accelerate.

The AFM images associated with the nucleated materials also provide for intriguing results depicted in Fig. 14. The center of the disc shows the ridges that are affiliated with individual CNCs dispersed in the polymer matrix [15]. The CNCs in this figure are not aligning to a specific direction of orientation, indicating that a strong shear force is not present at the 0* location. Polymer lamellae contributing to a superstructure are not seen in this image, indicating a fine, grainy structure has been developed during crystallization. When the nucleated material is subjected to a high level of shear (400 MPa, bottom row), both PA 12 lamellae and dispersed CNCs are oriented in the direction of flow. The lamellae in the nucleated material at the center of the sheared disc have an average width of approximately 22 ± 4 nm, and the lamellae at the edge of the disc, corresponding to 400 MPa, have lamellae ranging from approximately 20 ± 4 nm in width.

XRD measurements were also collected across the disc cross section to analyze any changes in polymorph due to shear. The scattering profiles are displayed in Fig. 15(a) corresponds to the neat PA 12 disc and Fig. 15b corresponds to the PA 12 nucleated with CNCs at intervals of increasing work. All analysis scans show two peaks at approximately 19 and 20.8 ° (2θ). These peaks are indicative of the α'-crystal formation, expected as a result of crystallization at low supercooling of the melt [7,48].

4. Conclusions

This study details the first investigation on the effects of flow-induced crystallization with a nano-composite polymeric material at process-relevant crystallization conditions. The use of a parallel plate rheometer as both a characterization device and a sample preparation tool allows for the development of samples with a very controlled shear history for subsequent calorimetric analyses. By using a novel methodology of staying below the equilibrium melting temperature, we were able to re-activate the flow-induced precursors that provide for accelerated crystallization.

The homogeneous-nucleation driven crystallization of neat PA 12 was impervious to previous shear flow, maintaining consistent crystallization kinetics throughout the homogeneous nucleation regime, between 65 and 95 °C. At temperatures greater than 95 °C, in the heterogeneous nucleation regime, the time required for crystallization decreased with increasing shear work. At the greatest specific work level studied, 400 MPa, unfilled PA 12 underwent the fastest crystallization rate, indicating that higher amounts of shear may yet increase the nucleation rate. Microstructure developed as a function of shear work in the unfilled PA 12, beginning at 0* MPa with a spherulitic, radial growth, and transitioning to oriented lamellae at high work levels.

When the PA 12 was nucleated with cellulose nanocrystals, the crystallization peak time in the heterogeneous nucleation regime decreased markedly, as anticipated judging by other studies available in the literature. Interestingly, when shear was applied to the composite CNC PA 12 system, it did not have an effect on the time required for isothermal crystallization below 140 °C. The nucleating effect of the nanoparticles was enough to saturate the system to the point that shear work up to 400 MPa would not further accelerate crystallization, except at very high crystallization temperatures (T > 140 °C). AFM studies of the composite microstructures revealed that, at different work levels in the CNC PA 12 material, different lamellar morphologies were developed. Specifically, the 0* MPa location at the center of the disc showed individual, unoriented CNCs dispersed in the material and a fine, grain structure was developed in the polymer phase. However, at high shear, oriented CNCs were identified and oriented lamellae were grown in the direction of flow, similar to that of the neat material.

Acknowledgments

The authors would like to thank Professor Christoph Schick for his colossal contributions to the field of thermal analysis, which have been exceedingly helpful and opened new doors of exploration for us since beginning FSC work at Penn State in 2014. In addition, Christoph has provided challenging, encouraging and insightful discussion on several occasions, which have undoubtedly spurred our work to a higher level of quality. For all of this, the authors are grateful. We also thank Jerry Magraw for assistance in NMR and GC–MS characterization of the base polymer.

This work was supported by the National Science Foundation under grant no. 1653629.

Appendix A. Supplementary data

Supplementary material related to this article can be found, in the online version, at doi:https://doi.org/10.1016/j.tca.2019.03.034.

References

[1] M.I. Kohan, Nylon Plastics Handbook, Hanser/Gardner, Cincinnati, 1995.
[2] J.S. Stansbury, M.J. Idacavage, 3D printing with polymers: challenges among expanding options and opportunities, Dent. Mater. 32 (1) (2016) 54–64.
[3] Stratsys, 18 December 2018. [Online]. Available: https://www.stratasys.com/materials/search/fdm-nylon-12. [Accessed 18 December 2018].
[4] N. Hiramatsu, K. Haraguchi, S. Hirakawa, Study of transformations among α, γ, and γ' forms in nylon 12 by X-ray and DSC, J. Appl. Phys. 22 (2) (1983) 335–339.
[5] T. Ishikawa, S. Nagai, The gamma to alpha partial transformation in nylon 12 by drawing, Makromolecular Chem. 182 (1981) 977–988.
[6] C. Ramesh, Crystalline transitions in nylon 12, Macromol. Commu. 32 (1999) 5704–5706.
[7] F. Paolucci, D. Baeten, P.C. Roozemond, B. Goderis, G.W.M. Peters, Quantification of isothermal crystallization of polyamide 12: modelling of crystallization kinetics and phase composition, Polymer 155 (2018) 187–198.
[8] A.M. Gohn, A.M. Rhoades, N. Wonderling, T. Tighe, R. Androsch, The effect of supercooling of the melt on the semicrystalline morphology of PA 66, Thermochim. Acta 655 (2017) 313–318.
[9] M. van Drongelen, T. Meijer-Vissers, D. Cavallo, G. Portale, G.V. Poel, R. Androsch, Microfocus wide-angle X-ray scattering of polymers crystallized in a fast scanning chip calorimeter, Thermochim. Acta 563 (2013) 33–37.
[10] A. Mollova, R. Androsch, D. Mileva, C. Schick, A. Benhamida, Effect of supercooling on crystallization of polyamide 11, Macromolecules 46 (3) (2013) 828–835.
[11] C. Fischer, A. Seefried, D. Drummer, Crystallization and component properties of polyamide 12 at processing-relevant cooling conditions, Polymer Eng. Sciencef (2017) 450–457.
[12] J. Sandler, S. Pegel, M. Cadek, F. Gojny, M. van Es, J. Lohmar, W.J. Blau, K. Schulte, A.H. Windle, M. Shaffer, A comparative study of melt spun polyamide-12 fibers reinforced with carbon nanotubes and nanofibers, Polymer 5 (2004) 2001–2015.
[13] B. Lecouvet, J. Gutierrez, M. Sclavons, C. Bailly, Structure-property relationships in polyamide 12/halloysite nanotube nanocomposites, Polym. Degrad. Stab. 96 (2011) 226–235.
[14] S. Chatterjee, N. F. A, C. B. T. T, Comparing carbon nanotubes and graphene nanoplatelets as reinforcements in polyamide 12 composites, Nanotechnology 22 (27) (2011) p. 275714.
[15] A. Nicharat, J. Sapkota, C. Weder, F. E. J, Melt processing of polyamide 12 and cellulose nanocrystals nanocomposites, J. Appl. Polym. Sci. 132 (45) (2015) 42752–42762.
[16] J. Marett, A. Aning, F. E. J, The isolation of cellulose nanocrystals from pistachio shells via acid hydrolysis, Ind. Crops Prod. 109 (2017) 869–874.
[17] S. Mueller, C. Weder, E.J. Foster, Isolation of cellulose nanocrystals from pseudostems of banana plants, RSC Adv. 4 (2) (2014) 907–915.
[18] M.M. de Souza Lima, R. Borsali, Rodlike cellulose microcrystals: structure, properties, and applications, Macromol. Rapid Commun. 25 (7) (2004) 771–787.
[19] D. Klemm, F. Kramer, S. Moritz, T. Lindstrom, M. Ankerfors, D. Gray, A. Dorris, Nanocelluloses: a new family of nature-based materials, Angew. Chemia Int. Ed. 50 (2011) 5438–5466.
[20] W.J. Orts, J. Shey, S.H. Imam, G.M. Glenn, M.E. Guttman, R. J. F, Application of cellulose microfibrils in polymer nanocomposites, J. Polym. Enviconment 13 (4) (2005) 301–306.
[21] H. Kargarzadeh, M. Mariano, J. Huang, N. Lin, I. Ahmad, A. Dufresne, S. Thomas, Recent developments on nanocellulose reinforced polymer nanocomposites: A review, Polymer 132 (2017) 368–393.
[22] C. Endes, S. Muller, O. Schmid, D. Vanhecke, E.J. Foster, A. Petri-Fink, B. Rothen-Rutishauser, C. Weder, M.J.D. Clift, Risk assessment of released cellulose nanocrystals - mimicking inhalatory exposure, J. Phys. Conf. Ser. 429 (2013).
[23] A. Sani, Y. Dahman, Improvements in the production of bacterial synathesized biocellulose nanofibers using different culture methods, J. Chem. Technol. Biotechnol. 85 (2) (2009) 151–164.
[24] J.E. Schawe, P. Pötschke, I. Alig, Nucleation efficiency of fillers in polymer crystallization studied by fast scanning calorimetry: carbon nanotubes in polypropylene, Polymer 116 (2017) 160–172.
[25] A.M. Gohn, A.M. Rhoades, D. Okonski, R. Androsch, Effect of melt-memory on the crystal polymorphism in molded isotactic polypropylene, Macromol. Mater. Eng. 303 (2018) 1–7.
[26] D.V. Rosato, D.V. Rosato, M.G. Rosato, Injection Molding Handbook, Springer, New York, 2000.
[27] B.N. Turner, R. Strong, S.A. Gold, A review of melt extrusion additive manufacturing processes: I. process design and modeling, Rapid Prototyp. J. 20 (3) (2014) 192–204.
[28] G.W.M. Peters, L. Balzano, R.J.A. Steenbakkers, "Flow induced crystallization", Handbook of Polymer Crystallization, John Wiley & Sons, Hoboken, NJ, 2013, pp. 399–433.
[29] J.-W. Housmans, R.J. Steenbakkers, P.C. Roozemond, G.W. Peters, H.E. Meier, Saturation of pointlike nuclei and the transition to oriented structures in flow-induced crystallization of isotactic polypropylene, Macromolecules 42 (15) (2009) 5728–5740.
[30] M. Okura, P. Chambon, O.O. Mykhaylyk, J.P.A. Fairclough, A.J. Ryan, Using multimodal blends to elucidate the mechanism of flow-induced crystallization in polymers, J. Polym. Sci. Part B: Polym. Phys. 49 (9) (2011) 621–628.
[31] H. Janeschitz-Kriegl, E. Ratajski, M. Stadlbauer, Flow as an effective promotor of nucleation in polymer melts: a quantitative evaluation, Rheol. Acta 42 (4) (2003) 355–364.
[32] O.O. Mykhaylyk, P. Chambon, R.S. Graham, J.P.A. Fairclough, P.D. Olmsted, The specific work of flow as criterion for orientation in polymer crystallization, Macromolecules 41 (6) (2008) 1901–1904.
[33] F.G. Hamad, R.H. Colby, S.T. Milner, Onset of flow-induced crystallization kinetics of highly isotactic polypropylene, Macromolecules 48 (2015) pp. 3752-3738.
[34] F.G. Hamad, R.H. Colby, S.T. Milner, Lifetime of flow-induced precursors in isotactic polypropylene, Macromolecules 48 (2015) 7286–7299.
[35] A.M. Rhoades, A.M. Gohn, J. Seo, R. Androsch, R.H. Colby, Sensitivity of polymer crystallization to shear at low and high supercooling of the melt, Macromolecules 51 (2018) 2785–2795.
[36] C.J.G. Plummer, J.-E. Bourban, J.-A.E. Månson, The crystallization kinetics of polyamide-12, Colloid Polym. Sci. 279 (2001) 312–322.
[37] S. Gogolewski, K. Czerniawska, M. Gasiorek, Effect of annealing on thermal properties and crystalline structure of polyamides. Nylon 12 (polylaurolactam), Colloid & Polymer Sci 258 (1980) 1130–1136.
[38] J. Seo, H. Takahashi, B. Nazari, A.M. Rhoades, R.P. Schaake, R.H. Colby, Isothermal flow-induced crystallization of polyamide 66 melts, Macromolecules 51 (2018) 4269–4279.
[39] H. Janeschitz-Kriegl, E. Ratajski, M. Stadlbauer, Flow as an effective promotor of nucleation in polymer melts: a quantitative evaluation, Rheol. Acta 42 (4) (2003) 355–364.
[40] K.A. Iyer, G.T. Schueneman, J.M. Torkelson, Cellulose nanocrystal/polyolefin biocomposites prepared by solid-state shear pulverization: superior dispersion leading to synergistic property enhancements, Polymer 56 (2015) 464–475.
[41] D. Bagheriasl, P.J. Carreau, B. Riedl, C. Dubois, W.Y. Hamad, Shear rheology of polylactide (PLA)-cellulose nanocrystal (CNC) nanocomposites, Cellulose 23 (3) (2016) 1885–1897.
[42] E. Piorkowska, G.C. Rutledge, Handbook of Polymer Crystallization, John Wiley & Sons, Inc, Hoboken, 2013.
[43] A.M. Rhoades, J.L. Williams, R. Androsch, Crystallization kinetics of polyamide 66 at processing-relevant cooling conditions and high supercooling, Thermochim. Acta 603 (2015) 103–109.
[44] I. Kolesov, R. Androsch, D. Mileva, W. Lebek, A. Benhamida, M. Kaci, W. Focke, Crystallization of a polyamide 11/organo-modified montmorillonite nanocomposite at rapid cooling, Colloid Polym. Sci. 291 (2013) 2541–2549.
[45] E. Zhuravlev, A. Wurm, P. Pötschke, R. Androsch, J.W.P. Schmelzer, C. Schick, Kinetics of nucleation and crystallization of poly(e-caprolactone) – multiwalled carbon nanotube composites, Eur. Polym. J. 52 (2014) 1–11.
[46] Y. Furushima, S. Kumazawa, H. Umetsu, A. Toka, E. Zhuravlev, A. Wurm, C. Schick, Crystallization kinetics of poly(butylene terephthalate) and its talc composites, J. Appl. Polym. Sci. 134 (16) (2016) 1–11.
[47] J. Seo, A.M. Gohn, O. Dubin, H. Takahashi, H. Hasegawa, R. Sato, A.M. Rhoades, R.P. Schaake, R.H. Colby, Isothermal crystallization of poly(ether ether ketone) with different molecular weights over a wide temperature range, Polym. Cryst. (2018).
[48] L. Li, M.H.J. Koch, W.H. de Jeu, Crystalline structure and morphology in Nylon-12: a small- and wide-angle X-ray scattering study, Macromolecules 36 (2003) 1626–1632.